Journal of Asian Earth Sciences 177 (2019) 275–286

Contents lists available at ScienceDirect

Journal of Asian Earth Sciences

journal homepage: www.elsevier.com/locate/jseaes

Full length article

Early Carboniferous metamorphism of the Neoproterozoic South Tien Shan-Karakum basement: New geochronological results from Baisun and Kyzylkum, Uzbekistan

D. Konopelko[a,b,*], Yu.S. Biske[a], K. Kullerud[c], I. Ganiev[d], R. Seltmann[e], W. Brownscombe[e], R. Mirkamalov[f], B. Wang[g], I. Safonova[b,h], P. Kotler[b,h], V. Shatov[i], M. Sun[j], J. Wong[j]

[a] St. Petersburg State University, 7/9 University Embankment, St. Petersburg 199034, Russia
[b] Novosibirsk State University, 1 Pirogova St., Novosibirsk 630090, Russia
[c] Norwegian Mining Museum, P.O. Box 18, 3602 Kongsberg, Norway
[d] National University of Uzbekistan, Department of Geology, Tashkent, Uzbekistan
[e] Natural History Museum, Centre for Russian and Central EurAsian Mineral Studies (CERCAMS), London SW7 5BD, UK
[f] Institute of Mineral Resources, Gozkomgeologiya, Tashkent, Uzbekistan
[g] State Key Laboratory for Mineral Deposits Research, Department of Earth Sciences, Nanjing University, Nanjing 210093, China
[h] Institute of Geology and Mineralogy, SB RAS, Koptyuga ave. 3, Novosibirsk 630090, Russia
[i] All Russian Geological Research Institute (VSEGEI), St. Petersburg 199106, Russia
[j] Department of Earth Sciences, The University of Hong Kong, Pokfulam Road, Hong Kong, China

ARTICLE INFO

Keywords:
Uzbekistan
South Tien Shan (Tianshan)
Baisun Block
Zircon ages
Neoproterozoic basement
Carboniferous metamorphism

ABSTRACT

Paleozoic evolution of the western Tien Shan, which is built up on the basement of the Karakum continent, is poorly constrained compared to the better investigated Tien Shan terranes along the margin of the Tarim Craton. We present magmatic, metamorphic and detrital zircon ages for the regionally metamorphosed Baisun block and the metasediments comprising the Karakum basement in the westernmost parts of the South Tien Shan terrane. Age spectra of detrital zircon from metasediments of the Baisun metamorphic block and the western South Tien Shan show remarkable similarities over the vast area extending for ca. 500 km and are characterized by major Neoproterozoic peak at 1200–600 Ma and smaller peaks at 2300–1700 and 2700–2400 Ma. The 570–540 Ma ages of the youngest grains define late Neoproterozoic (Ediacaran) – early Cambrian maximum depositional ages of the metasediments. Comparison of the obtained age spectra with those published for the adjacent Tien Shan terranes indicate that the detrital zircon grains in the studied Ediacaran sediments were derived from the southern Precambrian continents of Karakum and Tarim while transport from the Northern Tien Shan was limited. The age of the Barrovian metamorphism in the Baisun block is constrained by ages of anatectic granites in the range 352–340 Ma, corresponding to early Carboniferous. These ages well match the 340–330 Ma ages, established for the adjacent Lolabulak and Garm metamorphic blocks. Based on the regional distribution of suture zones we suggest that during the Carboniferous the relatively small tectonic blocks of the South Gissar comprised an archipelago, located between the larger continents of Karakum and Tarim and possibly connected with the Paleotethys Ocean. The archipelago scenario can explain hot and rapid metamorphic and tectonic processes, documented in the South Gissar, similar to the ongoing collision along the Australia – SE Asia junction.

1. Introduction

The Tien Shan orogen is situated in the southern part of the Central Asian Orogenic Belt (Fig. 1), and was formed by the late Paleozoic (Hercynian) collision between the Precambrian continents of Karakum and Tarim in the south and the early Paleozoic Kazakhstan continent in the north (Zonenshain et al., 1990; Şengör et al., 1993; Windley et al., 2007; Biske and Seltmann, 2010; Biske et al., 2013; Burtman, 2015; Cai et al., 2018). While the Hercynian events at the Tarim margin are relatively well investigated, much less is known about the evolution of the westernmost Tien Shan belt, which is built up on the basement of the Karakum continent. The characteristic features of the western Tien

* Corresponding author at: Geological Faculty, St. Petersburg State University, 7/9 University Embankment, St. Petersburg 199034, Russia.
E-mail addresses: d.konopelko@spbu.ru, konopelko@inbox.ru (D. Konopelko).

https://doi.org/10.1016/j.jseaes.2019.03.025
Received 13 November 2018; Received in revised form 17 March 2019; Accepted 31 March 2019
Available online 03 April 2019

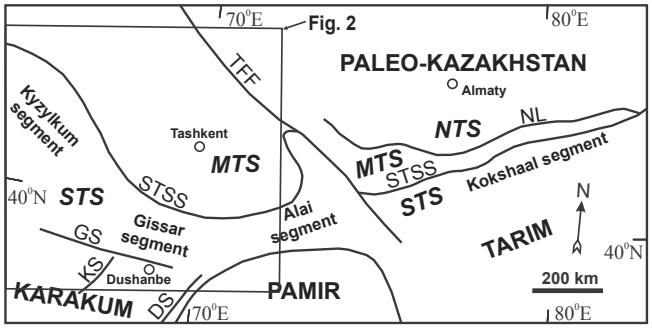

Fig. 1. Principal terranes of the south-western Central Asian Orogenic Belt. Based on Burtman (2012), modified by the authors. Abbreviations: *NTS* – Northern Tien Shan, *MTS* – Middle Tien Shan, *STS* – South Tien Shan, NL – Nikolaev Line, TFF – Talas-Fergana Fault, STSS – South Tien Shan Suture, GS – Gissar Suture, KS – Kundajuaz Suture, DS – Darvaz Suture.

Shan and Karakum, distinguishing these terranes from the Tarim margin, include the Barrovian metamorphic complexes and a number of Paleozoic suture zones dissecting the northern Karakum margin. In this paper we present magmatic, metamorphic and detrital zircon ages for the regionally metamorphosed Baisun block and the metasediments composing the basement of the Kyzylkum segment of the western South Tien Shan. The obtained results allow us to elucidate the timing of Barrovian metamorphism and the age and the provenance of clastic sedimentary rocks at the Karakum margin, thus, providing important geochronological piercing points for the poorly constrained geodynamic evolution of the westernmost Tien Shan in Uzbekistan.

2. Principal tectonic units of western Tien Shan

The western Tien Shan is composed of three major tectonic units or terranes: the Northern Tien Shan (NTS), the Middle Tien Shan (MTS) and the South Tien Shan (STS) (Popov, 1938; Zonenshain et al., 1990; Biske and Seltmann, 2010; Burtman, 2012, 2015). These east-west trending linear terranes are cut by the NW trending Talas-Fergana Fault with a total dextral offset of about 200 km (Figs. 1 and 2). The NTS is represented by the early Paleozoic continental arc formed on the southern margin of the Paleo-Kazakhstan continent as a result of northward subduction and subsequent closure of the Terskey Ocean during late Ordovician (Lomize et al., 1997; Ghes, 2008). The main component of the MTS is the Chatkal-Kurama terrane, a late Paleozoic continental arc formed during the evolution and closure of the Turkestan Ocean to the south. The MTS and STS are separated by the Southern Tien Shan Suture. The STS represents a pile of folded tectonic nappes, which are thrust southward upon the passive margin of the Karakum-Tarim continent during closure of the Turkestan Ocean in late Carboniferous. The STS is traditionally divided into 4 segments from west to east: the Kyzylkum, Gissar, Alai and Kokshaal segments (Fig. 1).

3. The Gissar segment of South Tien Shan

The northern part of the Karakum continent is dissected by several major faults separating the tectonic units, which developed in different geodynamic settings. The Gissar segment of STS, built up on the northern Karakum margin, consists of four units (Fig. 3). The Nuratau-Turkestan unit comprises folded Paleozoic formations thrust to the south over the Precambrian Zeravshan-Alai block. The presence of shallow level Cambrian carbonates indicates that during the earliest Paleozoic this block developed as a passive margin of the Turkestan Ocean. (Biske, 1996). The passive margin formations are overlain by Ordovician and Silurian turbidites and volcaniclastics of arc affinity. The arc complex is unconformably overlain by Devonian - Carboniferous carbonate platforms and middle Carboniferous (Moscovian) flysch, which are overthrust by the nappes composed of ophiolites.

The Zeravshan-Alai block docked with the Karakum continent during late Paleozoic after the closure of the inferred middle Paleozoic oceanic Vashan basin. The ophiolite-marked Zeravshan suture separating the Zeravshan-Alai block from the Karakum continent is exposed further west in the Kyzylkum segment of STS. The Vashan unit, composed of late Paleozoic bathyal sediments, presumably represents a residual foreland belt formed on the eastern continuation of the Zeravshan suture.

The Zeravshan-Gissar unit, located to the south of the Zeravshan suture, represents the northern margin of the Karakum continent, which was significantly reworked during the Hercynian collision. The basement is not exposed and its age is constrained by the Neoproterozoic Nd model ages of crosscutting late Paleozoic granites (Konopelko et al., 2015, 2018; Käßner et al., 2017; Worthington et al., 2017). The Paleozoic formations include Ordovician to Devonian clastics and carbonates unconformably overlain by lower Carboniferous

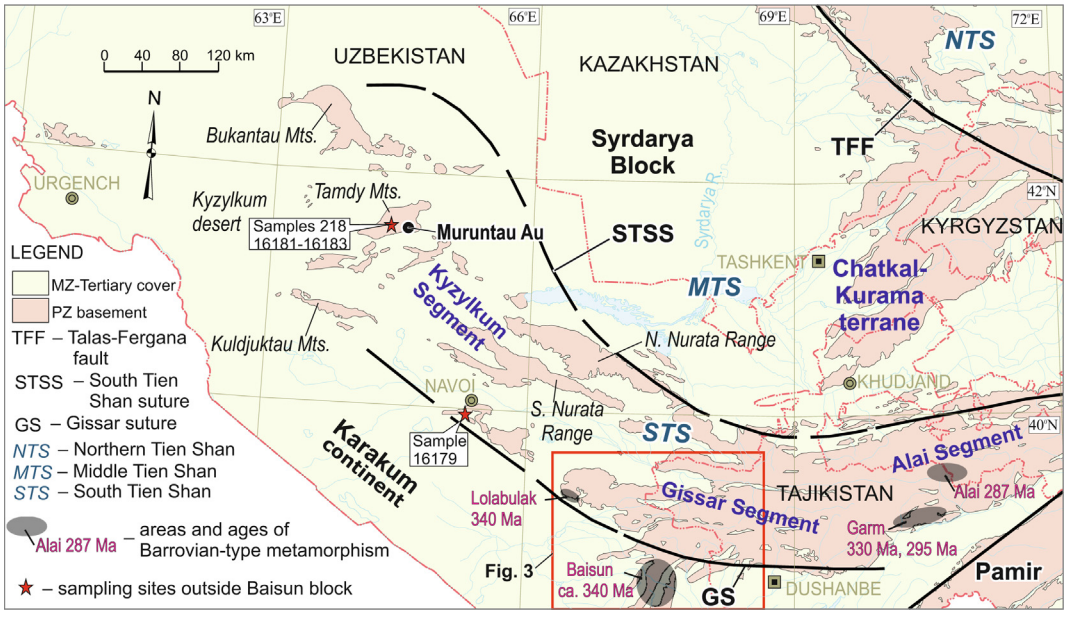

Fig. 2. Overview map of the western Tien Shan showing major tectonic subdivisions and areas of Barrovian metamorphism.

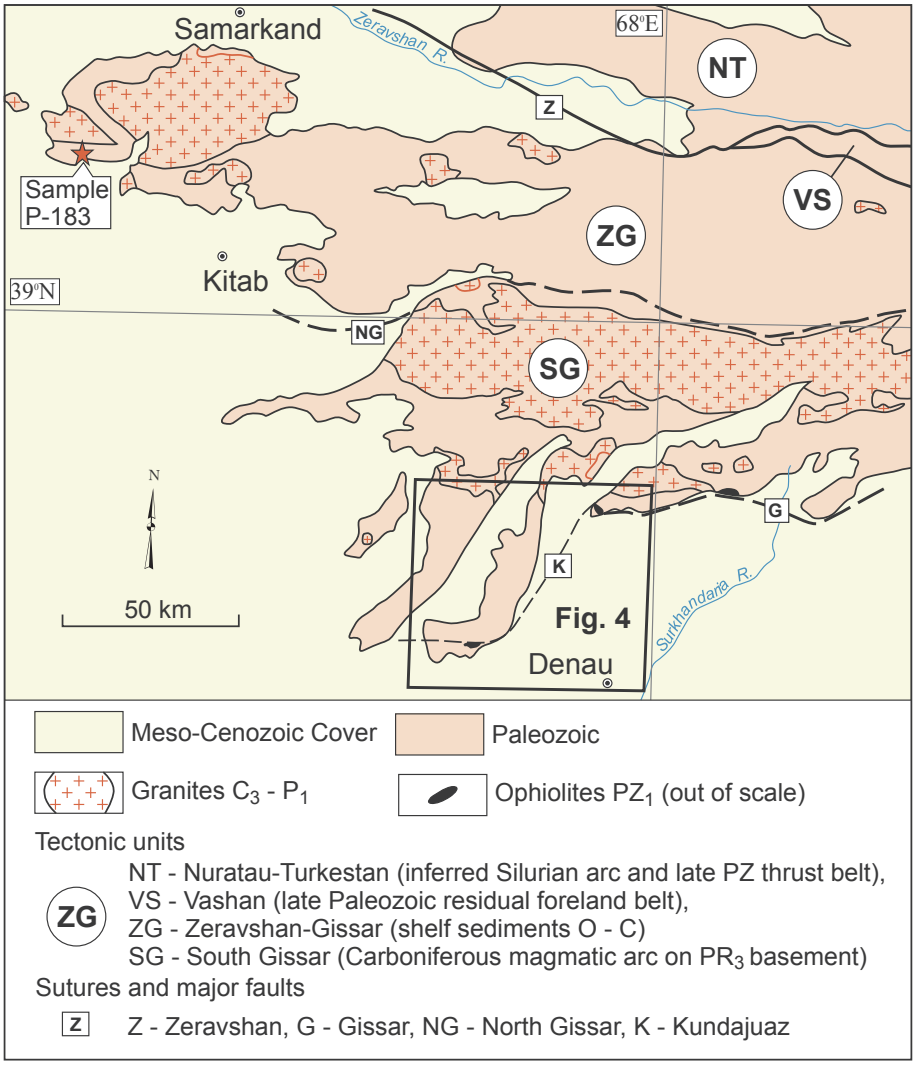

Fig. 3. Tectonic units of the Gissar Segment of South Tien Shan and sampling site within the Lolabulak metamorphic block.

turbidites and middle Carboniferous limestones. The Fan-Karategin belt of greenschist-facies metabasalts and related sediments with ages varying from of 590 to 450 Ma (Volkova and Budanov, 1999; Worthington et al., 2017) is located in the southern part of the Zeravshan-Gissar unit.

The South Gissar unit is separated from the northern terranes by the major North Gissar fault. A significant part of the South Gissar unit is occupied by the Baisun metamorphic block, which has been interpreted as an uplifted basement of the Karakum continent (Akhmedjanov et al., 1975; Baratov, 1976; Vlasov et al., 1991). The early-middle Paleozoic cover of the South Gissar is similar to that of the Zeravshan-Gissar unit. However, in contrast to the Zeravshan-Gissar, the South Gissar unit is characterized by voluminous Carboniferous magmatism, presumably related to a northward subduction in a short-lived Gissar basin as suggested by remnants of oceanic crust preserved in the Gissar and Kundjuaz suture zones (Fig. 4). The Turkestan Ocean and smaller basins to the south were closed in the course of Hercynian collision during late Carboniferous – early Permian. Voluminous early Permian post-collisional magmatism affected all parts of Tien Shan across terrane boundaries.

4. Barrovian type metamorphic complexes of the South Tien Shan

Although the Paleozoic formations of STS generally lack tectonic features characteristic for high-grade regional continental metamorphism, there are four Barrovian type metamorphic complexes in the Gissar segment, which are known in the literature as the Lolabulak, Baisun, Garm and Alai metamorphic blocks (Fig. 2) (Bukharin et al., 1985). Another occurrence of early Permian high-grade rocks was recently described further east in the Kokshaal segment by Loury et al. (2018). The metamorphic conditions of the four blocks in the Gissar segment vary from greenschist- to amphibolite-facies. The amphibolite-facies rock assemblage, including variably migmatized biotite ± staurolite ± sillimanite ± cordierite ± garnet gneisses, is characteristic for medium P/T amphibolite-facies metamorphic complexes typical for regional Barrovian type metamorphism in orogenic belts. All four metamorphic blocks are located in the South Gissar unit (Figs. 2 and 3).

Geochronology and metamorphic petrology of the Garm block was recently addressed by Konopelko et al. (2015), Käßner et al. (2017) and Worthington et al. (2017). These authors have shown that the youngest zircon grains with ages around 550 Ma consistently define Ediacaran maximum depositional ages of the sedimentary protoliths of the Garm metamorphic rocks. The main peak of the amphibolite-facies metamorphism was proved to be about 290 Ma, corresponding to the early Permian. However, metamorphic zircon grains with ca. 330 Ma ages, registered in various rock types, indicate an earlier metamorphic event. The ca. 330 Ma age, obtained for the earlier metamorphic episode in Garm, is similar to an age of ca. 340 Ma, reported for HT-LP metamorphism in the Lolabulak block by Mirkamalov et al. (2012). The

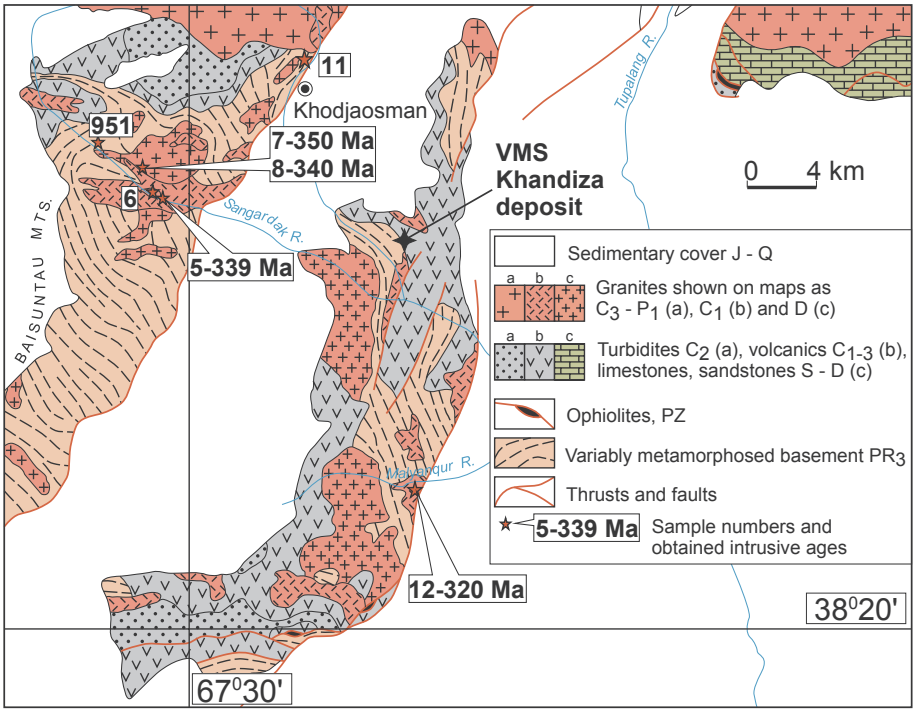

Fig. 4. Schematic geological map of the Baisun metamorphic block. Modified from the 1:500 000 geological map of Uzbekistan (Shayakubov, 1998).

easternmost Alai block is poorly studied. An age of 287 ± 4 Ma (U-Pb zircon, Konopelko et al., 2018), obtained from a granodiorite of the Liayliak massif, which was emplaced in migmatized gneisses, is indistinguishable from ca. 290 Ma age of peraluminous granitoids that were emplaced coevally with the amphibolite-facies metamorphism in the Garm block (Konopelko et al., 2015; Worthington et al., 2017).

5. Geology of the Baisun metamorphic block and sampling

The Baisun metamorphic block makes up the southern part of the South Gissar unit that was displaced by Cenozoic dextral strike-slip motions relative to the uplifted northern part of this unit exposed in the Gissar range (Fig. 3). Pre-Mesozoic formations of the Baisun block outcrop within several large NE-striking tectonic slivers, separated by thrusts, and comprise metamorphosed basement overlain by late Paleozoic sediments and volcanics (Fig. 4).

The metamorphic basement rocks, described as the Baisuntau Supergroup of inferred Proterozoic age, comprise variably metamorphosed clastic sediments (mostly mudstones and sandy turbidites) intercalated with volcaniclastics and minor limestones (Baratov, 1976; Bukharin et al., 1985; Shayakubov and Dalimov, 1998; Abduazimova, 2001). The metamorphic conditions of the Baisuntau Supergroup rocks vary from greenschist- to amphibolite-facies. An outcrop photograph of a relatively low-grade metasandstone, sampled for geochronological investigations near the Khodjaosman village (sample 11), is given in Fig. 5c. The high-grade rocks, outcropping in the Sangardak river valley, comprise aluminous schists, quartzites and biotite ± sillimanite ± cordierite ± garnet gneisses with lenses of garnet amphibolite (Baratov, 1976; Bukharin et al., 1985). This rock assemblage is characteristic for continental regionally metamorphosed Barrovian type orogenic belts. Photographs of deformed and migmatized banded paragneisses, similar to those sampled for geochronology (sample 921), are given in Fig. 5a and b.

The metamorphic basement is crosscut by granites with poorly defined ages. The granites can be subdivided into three groups (Devonian, Carboniferous and late Carboniferous – early Permian, see Fig. 4). The granites, which are shown on geological maps as Devonian and

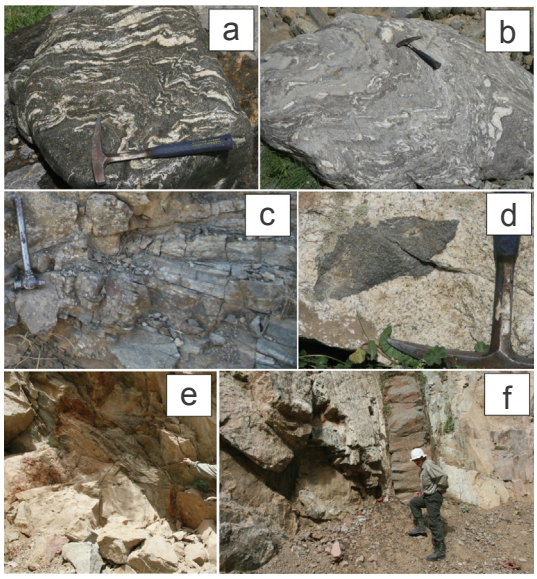

Fig. 5. Outcrop photographs from the Baisun metamorphic block: (a and b) amphibolite facies migmatized banded paragneisses, (c) low-grade metasandstone (sample 11), (d) close up view of metasandstone xenolith in granite, (e) xenoliths of paragneisses in anatectic granite, (f) mafic dike crosscutting granite (sample 5). Photographs a, b, e, f were taken in the upper part of Sargandak valley, c and d – close to the Khodjaosman village.

Carboniferous, comprise two series including small bodies of anatectic granites associated with migmatites in areas of high-grade metamorphism and larger intrusions, such as Vakhshivar massif in the central part of the Baisun block (Fig. 4). Both series consist of strongly peraluminous muscovite or biotite-muscovite leucogranites with accessory garnet and cordierite and numerous xenoliths of gneisses and schists (Fig. 5d and e) (Baratov, 1976). Anatectic granites associated with migmatized gneisses in the Sargandak river valley are represented by samples 6, 7 and 8. Sample 5 was collected from an undeformed mafic dike crosscutting the anatectic granites and possibly representing

a feeding channel for the overlying volcanics of the Vakhshivar Fm. (Baratov, 1976) (Fig. 5f).

The third series comprise relatively small subvolcanic bodies varying in composition from dacite to rhyolite and quartz porphyry. The rocks are characterized by porphyritic textures and moderately peraluminous compositions with increased alkalinity. In contrast to the anatectic granites, which do not show any crosscutting relationships with the overlying late Paleozoic formations, the subvolcanic bodies of the third series crosscut the lowermost of the overlying late Paleozoic formations, namely the early Carboniferous (Tournaisian-Visean) Zoi Fm., and are thought to be comagmatic with the thick volcanic piles of the Visean-Serpukhovian Vakhshivar Fm. that conformably overly the Zoi Fm. (Baratov, 1976; Abduazimova, 2001; Golovanov, 2001). The third series is represented by a monzodiorite of the Ushor intrusion (sample 12, Fig. 4).

The Zoi and Vakhshivar Fms. comprise the lowermost units of the late Paleozoic cover with basal conglomerates unconformably overlying the metamorphic basement. Thick (up to 2000 m) volcanic piles of these formations, presumably related to the opening of the Gissar rift (Burtman, 2015), host a number of volcanic massive sulfide (VMS) occurrences including the world-class Zn-Pb-Cu-Ag Khandiza deposit (Golovanov, 2001; Herrington et al., 2005). The Vakhshivar volcanics are unconformably overlain by the Middle Carboniferous (Bashkirian-Moscovian) turbidites, late Carbonifeorus marine molasses and early Permian volcanics.

In order to better represent the basement of the Karakum continent, several samples were collected in the Kyzylkum segment of STS west of the Baisun block (Fig. 2). Three samples (16,179, 16,181 and 16,182) were collected from metasedimentary formations that are relatively strongly metamorphosed compared to the surrounding rocks. These rocks have been described as gneisses and interpreted to represent an ancient basement (Baratov, 1976; Shayakubov, 1998); however, our field observations and petrographic studies have shown that the metamorphic grade probably did not exceed the greenschist-facies conditions.

Sample 16,179 was collected from the Kattarmai Fm. that forms a large (ca. 25 × 10 km) lens south of the town Navoi in the Zirabulak mountains (Fig. 3). The Kattarmai and adjacent formations are built up of typical metamorphosed oceanic crust, probably representing the western continuation of the Fan-Karategin belt of metabasalts. The Kattarmai Fm. is composed of quartz - plagioclase - muscovite ± chlorite ± epidote ± actinolite schists with amphibolite lenses intercalated with minor quartzites and marbles (Baratov, 1976). Outcrop photograph of typical greenschist-facies metasediments with amphibolite layer and a photograph of mica schist (sample 16,179), utilized for geochronological investigation, are given in Fig. 6a and b, respectively.

Samples 16,181 and 16,182 represent mica schists from the Djurgantau and Uchkuduktau Fms., respectively, which together with metamorphosed cherts of the Taskazgan Fm. were interpreted to represent the lowermost stratigraphic levels of the Caledonian basement in the Kyzylkum desert (Baratov, 1976). The Djurgantau and Uchkuduktau Fms. are composed of mica schists intercalating with quartzites and minor amphibolites (Fig. 6c). The two samples (16,181 and 16,182), collected from these formations, represent compositionally similar quartz – plagioclase – muscovite – biotite schists (Fig. 6d). Sample 218 represents relatively fresh metabasalt from the Uchkuduktau Fm. (Fig. 6e). In contrast to other samples of ortoamphibolite, from which no zircon grains were recovered, this sample produced a homogeneous population of magmatic zircon that was used for geochronology. Finally, because similar basalts are widespread upsection in the adjacent late Paleozoic formations, we also sampled a diabase dike crosscutting pillow basalts of the Elemesashchy Fm. (sample 16,183), which demonstrate baked contact with the late Paleozoic limestones (Fig. 6f and g). Dolgopolova et al. (2017) gave a geological description of the Tamdytau mountains, where the Kyzylkum samples were collected.

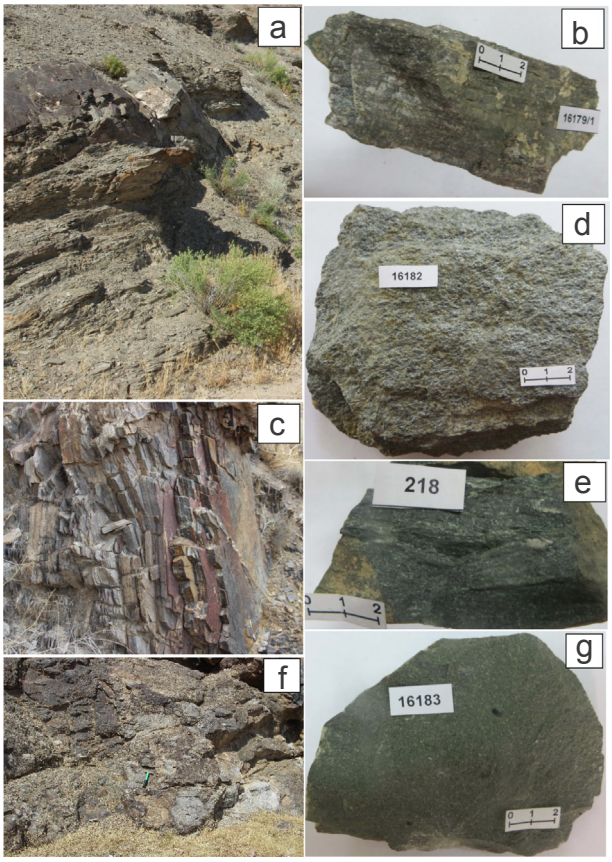

Fig. 6. Photographs of outcrops and samples from Kyzylkum area: (a) greenschist-facies metasediments of the Kattarmai Fm. with amphibolite layer, (b) mica schist from the Kattarmai Fm. (sample 16,179), (c) quartzites intercalating with mica schists in the Djurgantau Formation, (d) mica schist from the Uchkuduktau Fm. (sample 16,182), (e) metabasalt from the Uchkuduktau Fm. (sample 218), (f) debris of upper Paleozoic limestone filling the fracture in pillow basalts of the Elemesashchy Fm., (g) basalt from the Elemesashchy Fm. (sample 16,183).

6. Results

Zircon grains from 12 samples have been dated by LA-ICP-MS at the Universities of Hong Kong (samples 6, 7, 12, 218, 951, 16,182, 18,183) and Nanjing (16,179, 16,181), China and at the Kraków Research Centre, Poland (5, 8, 11). Details of the analytical procedures are given in Appendix A. The U–Pb analytical data and calculated ages are presented in the Supplementary Tables 1–3. Spot dating of zircon grains younger than about 1000 Ma is best achieved by using $^{206}Pb/^{238}U$ ages (Black and Jagodzinski, 2003), whereas $^{207}Pb/^{206}Pb$ ages are better constrained for zircon older than 1000 Ma due to the short half-life of ^{235}U producing ^{207}Pb (Black et al., 2003). This practice was adopted for reporting the obtained ages. Cathode luminescence (CL) images of representative analyzed zircon grains are shown together with concordia diagrams and probability density plots in Figs. 7–9.

The low-grade metasandstone from the Baisun metamorphic block (sample 11) produced ca. 50 variably rounded elongate detrital zircon grains. Eighteen spots in zircon were analyzed in this sample. Ten grains yielded Neoproterozoic ages in the range 720–575 Ma, while the other eight grains yielded Archean to Paleoproterozoic ages in the range 2700–2400 Ma. CL images of the analyzed Neoproterozoic and Archean zircon grains are shown in Fig. 7a. The ages of detrital zircon grains from sample 11 are presented on probability plots and histograms together with ages of detrital and xenogenic zircons from

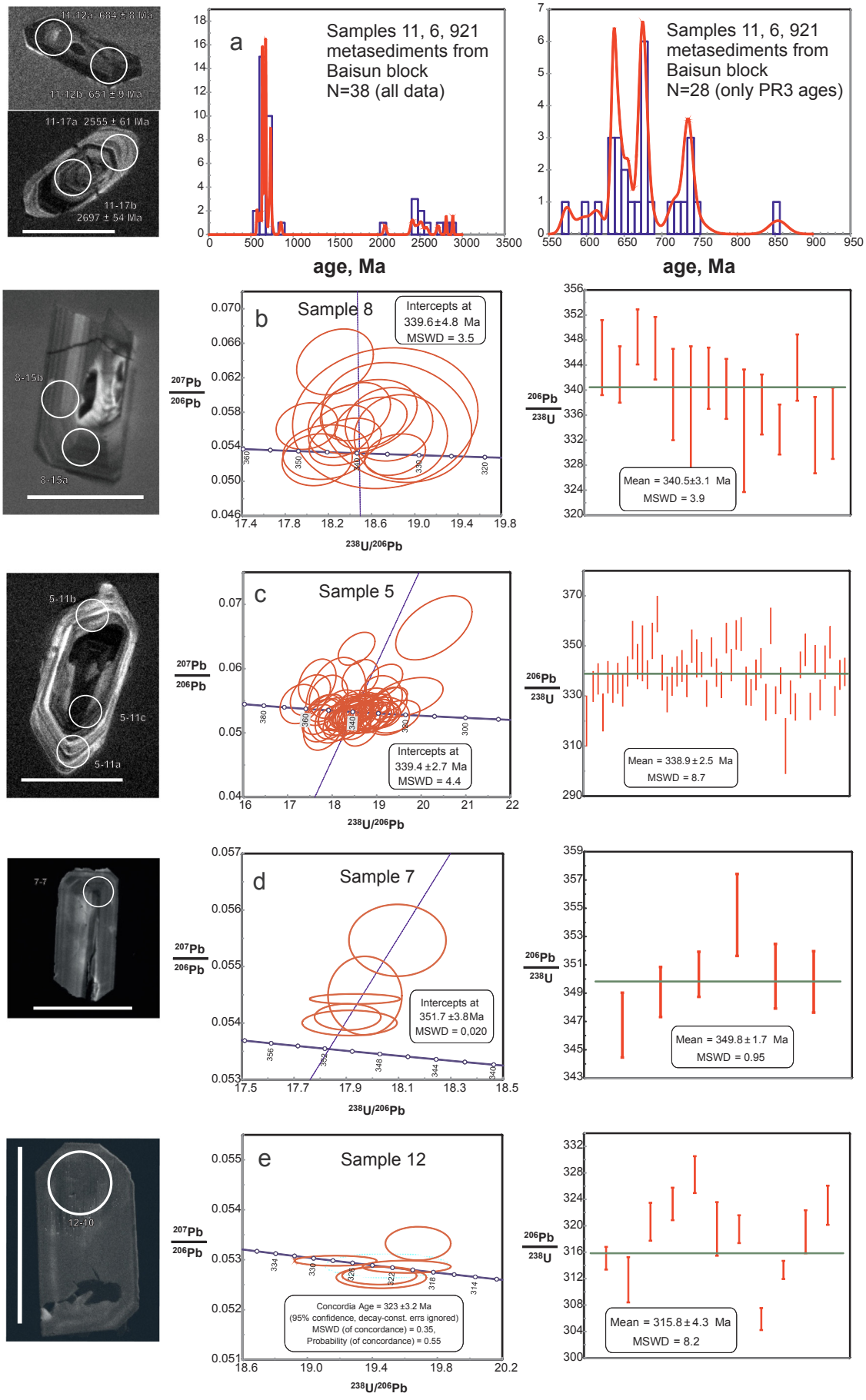

(caption on next page)

Fig. 7. Representative CL images of analyzed zircon grains and U-Pb analytical data for samples from the Baisun metamorphic block: (a) probability plots and histograms showing distribution of detrital zircon ages from metasediments, (b–e) concordia diagrams and weighted average $^{206}Pb/^{238}U$ ages for zircon U–Pb data of magmatic rocks. White bar on CL images corresponds to 0.1 mm.

samples 951 and 6, which produced similar age spectra (Fig. 7a). As seen on a plot for Neoproterozoic ages, presented on Fig. 7a separately, the youngest grains give ages of ca. 570 Ma, which constrains a latest Neoproterozoic Ediacaran maximum depositional age for the sedimentary protoliths of the metamorphic basement rocks of the Baisun block.

A relatively high-grade gneiss (sample 951) and a muscovite granite, sampled close to contact with gneiss (sample 6) in the Baisun metamorphic block, produced inhomogeneous populations of rounded grains, interpreted to be detrital and/or xenogenic. Eleven analytical spots on zircon grains from gneiss sample 951 yielded ages in the range 737–635 Ma. Nine spots were analyzed in zircon grains from sample 6. Seven analyses yielded similar Neoproterozoic ages in the range 678–638 Ma and 2 analyses yielded discordant ages of ca. 2.9 Ga. The ages of zircon grains from samples 6 and 951 are presented on probability plots and histograms together with ages of detrital zircon grains from sample 11 (Fig. 7a) and discussed above.

Anatectic granite from the Baisun metamorphic block (sample 8) produced a homogeneous population of stubby prismatic zircon grains with distinct facets and well pronounced magmatic zoning (Fig. 7b). Seventeen spots, analyzed in zircon grains from sample 8, yielded ages in the range 357–305 Ma. Most of the analytical data are slightly normally discordant. If one youngest and two oldest discordant analyses are excluded from the calculations, the remaining 15 analyses form a

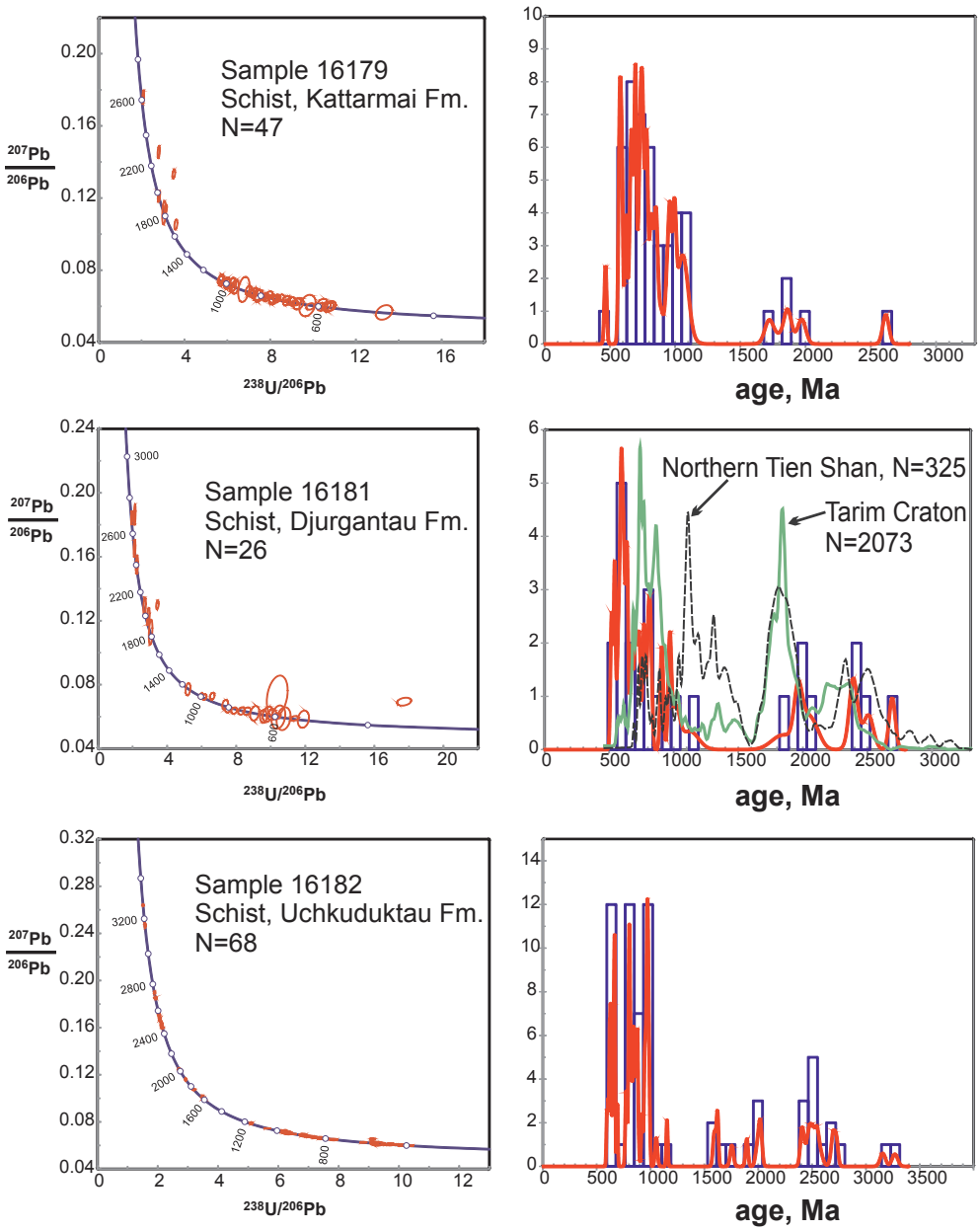

Fig. 8. Concordia diagrams and probability plots with histograms showing the distribution of detrital zircon ages from the Kyzylkum schists. Probability curves of detrital and magmatic zircon ages (mostly from Precambrian and lower Paleozoic rocks) from the Tarim Craton and the Northern Tien Shan, compiled by Rojas-Agramonte et al. (2014), are shown for comparison (not to vertical scale).

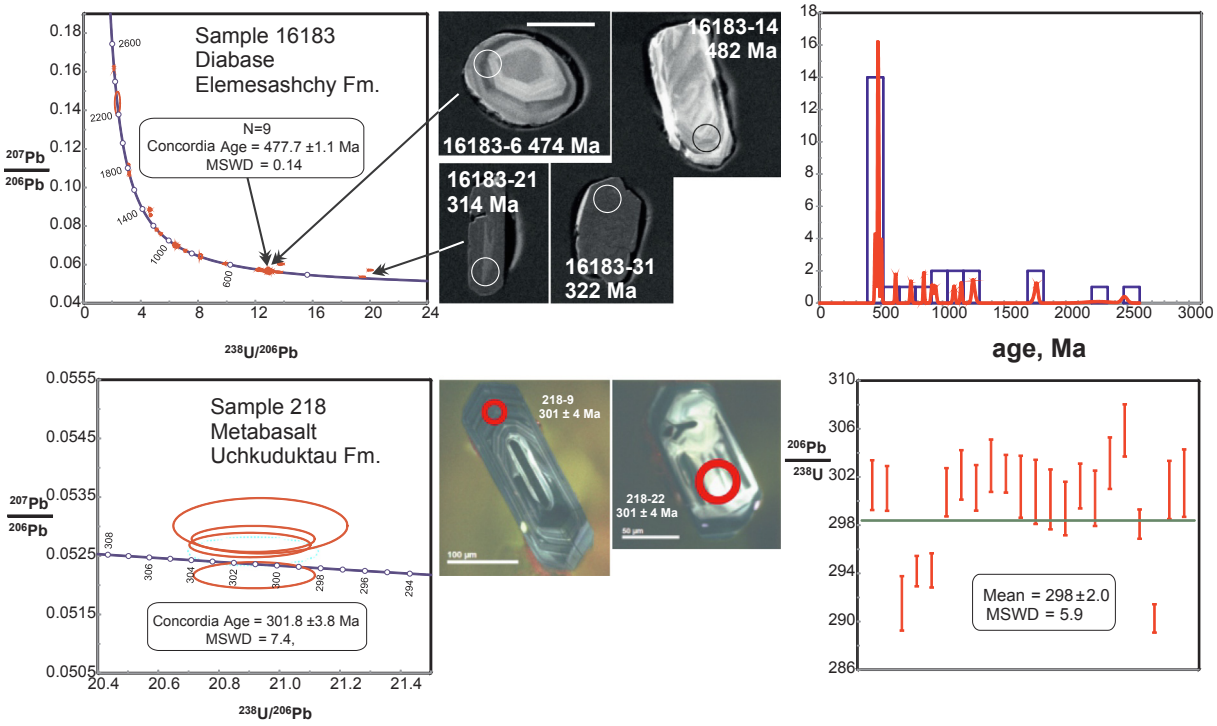

Fig. 9. Representative CL images of analyzed zircon and U-Pb analytical data for basalt samples from northern Kyzylkum.

relatively tight cluster and yield an intercept age of 340 ± 5 Ma (MSWD = 3.5) that is consistent with a weighted average age of 340 ± 3 Ma (MSWD = 3.9) (Fig. 7b). Thus, an age of 340 Ma is interpreted as a good estimate of crystallization age of the red granite.

A mafic porphyritic dike crosscutting the gneisses in the Baisun metamorphic block (sample 5) produced a homogeneous population of large elongate prismatic zircon grains with distinct facets and well pronounced magmatic zoning (Fig. 7c). Sixty-three spots, analyzed in zircon grains from sample 5, form a relatively wide cluster of concordant and slightly normally discordant data with ages in the range 360–320 Ma. If the four youngest and four oldest discordant outliers are excluded from the calculations, the remaining 55 analyses yield an intercept age of 339 ± 3 Ma (MSWD = 4.4), which is consistent with a weighted average age of 339 ± 2 Ma (MSWD = 8.7) (Fig. 7c), interpreted as the crystallization age of the mafic dike.

A dike of grey porphyritic granite (sample 7) of the Baisun metamorphic block produced a homogeneous population of elongate prismatic zircon grains with distinct facets and weak oscillatory zoning (Fig. 7d). However, due to technical problems only six spots were analyzed in zircon grains from this sample. The obtained data are variably discordant and yield a weighted average age of 350 ± 2 Ma (MSWD = 0.95), which is consistent with an intercept age of 352 ± 4 Ma (MSWD = 0.02) calculated for 5 normally discordant analyses (Fig. 7d). Due to insufficient number of analyses, an age of ca. 350 Ma is considered as a preliminary estimate of the (maximum) crystallization age of the grey porphyritic granite.

Monzodiorite from the Baisun metamorphic block (sample 12) produced a homogeneous population of stubby prismatic zircon grains with distinct facets. On CL images, the grains are characterized by dark colour and weak magmatic zoning. Eighteen spots, analyzed in zircon grains from sample 12, yielded variably normally discordant ages in the range 327–289 Ma. The five oldest concordant analyses form a cluster for which a concordia age of 323 ± 3 Ma (MSWD = 0.35) can be calculated (Fig. 7e). If the seven youngest discordant data are excluded from the calculation, the remaining eleven analyses yield a weighted average age of 316 ± 4 Ma (MSWD = 8.2). This relatively poorly defined age of ca. 320 Ma is considered as a preliminary estimate of the (maximum) crystallization age of the monzodiorite.

Mica schist from the Kattarmai Fm. (sample 16,179) produced ca. 100 rounded zircon grains typical for detrital zircon. Forty-seven spots, analyzed in zircon grains from sample 16,179, yielded ages in the range 2600–467 Ma with 2 major overlapping peaks at 900–570 and 1100–900 Ma and few ages in the range 2300–1700 Ma (Fig. 8). Several youngest grains with ages of ca. 570 Ma suggest a latest Neoproterozoic Ediacaran maximum depositional age of the sedimentary protolith of sample 16,179. However, the presence of one grain with an age of 467 Ma may indicate that the Kattarmai Formation has an Ordovician age. This suggestion is in agreement with the Ordovician age of the Kattarmai Formation indicated on regional geological maps (e.g. Shayakubov, 1998) and with an age of ca. 450 Ma, obtained by Worthington et al. (2017) for metavolcanics from compositionally similar formations of the Fan-Karategin belt located in the eastern part of the Gissar segment of STS.

Mica schist from the Djurgantau Fm. (sample 16,181) produced large amount of small rounded grains, ca. 10–20 μm in size, from which about 30 largest grains were picked and mounted for analysis. Twenty-six spots, analyzed in zircon grains from sample 16,181, yielded ages in the range 2700–520 Ma with major peak at 950–520 and smaller peak at 1200–900 Ma and few ages in the range 2700–1700 Ma (Fig. 8). Several youngest grains with ages of ca. 540–520 Ma suggest an early Cambrian maximum depositional age of the sedimentary protolith of sample 16,181.

Mica schist from the Uchkuduktau Fm. (sample 16,182) produced ca. 80 relatively big slightly elongate rounded grains typical for detrital zircon. Seventy seven spots were analyzed in zircon grains from sample 16,182. Nine discordant analyses were excluded from data presentation. The remaining 68 concordant analyses, presented in Table S1, yielded ages in the range 3200–600 Ma. On probability plots and histograms (Fig. 8) the ages show 3 major Neoproterozoic peaks at 600–700 Ma, 780–900 Ma and 920–1000 Ma and smaller peaks between 1500 and 2000 Ma and 2500–2700 Ma. The youngest ages of ca. 600 Ma suggest a latest Neoproterozoic Ediacaran maximum depositional age of the sedimentary protolith of sample 16,182.

Ca. 30 zircon grains, recovered from a diabase dike crosscutting

pillow basalts of the Elemesashchy Fm. (sample 16,183), comprised a very inhomogeneous population typical for xenogenic zircon and included grains of different shapes and sizes varying from large completely rounded grains to relatively well shaped smaller elongate transparent grains. Twenty nine spots analyzed in zircon grains from sample 16,183 yielded concordant or slightly discordant ages in the range 2477–314 Ma. Lower Paleozoic and Proterozoic ages of xenogenic zircon grains in the range 500–1550 form a major peak similar to late Proterozoic peaks characteristic for detrital zircon grains from metasedimentary rocks elsewhere in the Kyzylkum and Gissar segments of STS (cf. Mirkamalov et al., 2012; Konopelko et al., 2015). However, the presence of xenogenic rounded zircon grains with ages in the range 490–450 Ma (Fig. 9) is a unique feature of the Elemesashchy basalt. These ages are similar to the age of 438 Ma, obtained for adjacent Teskuduk ophiolite by Dolgopolova et al. (2017), and provide additional information on the ages of ophiolites, associated with the early stages of the evolution of the Turkestan Ocean. Finally, because the Elemesashchy basalts demonstrate baked contacts with Upper Paleozoic limestones (Fig. 9), we interpret the two youngest ages of 322 and 314 Ma, obtained for small well-shaped zircon grains (Fig. 9), as a preliminary estimate of the age of the diabase dike and as maximum crystallization age of the Elemesashchy basalts.

In contrast to the diabase dike associated with the Elemesashchy basalts, a metabasalt from the Uchkuduktau Fm. of inferred Neoproterozoic age (sample 218), produced a homogeneous population of zircon comprising ca. 30 transparent elongate prismatic grains with distinct facets and pronounced oscillatory zoning (Fig. 9). Twenty five spots were analyzed in zircon grains from sample 218. One xenogenic zircon yielded an age of 803 Ma. The remaining 24 analyses yielded similar ages in the range 306–288 Ma. However, most of analytical data are variably normally discordant (Table S1). If the two youngest discordant analyses are excluded from calculations, the remaining 22 analyses yield a weighted average age of 298 ± 2 Ma (MSWD = 5.9) that is indistinguishable from concordia age of 302 ± 4 Ma (MSWD = 7.4), calculated for the four most concordant analyses (Fig. 9). Because sample 218 produced a homogeneous population of magmatic zircon, we interpret the age of 302 Ma as a good estimate of the crystallization age of the deformed basalt from the Uchkuduktau Fm.

7. Discussion

7.1. Age of the South Tien Shan – Karakum basement

It is generally accepted that western segments of STS are built up on the Precambrian basement of the Karakum continent (Fig. 1) (Biske, 1996). Remarkable similarities of detrital zircon age spectra over the vast region of western STS were first recognized by Konopelko et al. (2015) based on the data for Neoproterozoic metasediments of the Garm block and the Kyzylkum segment of STS. Their conclusion is in agreement with results from Käßner et al. (2017) and Worthington et al. (2017) for the Garm block and the results presented here.

Three metasediment samples from the Baisun block and three metasediments sampled further west in the Kyzylkum segment of STS yielded similar detrital zircon age spectra with major peak observed between 1200 and 550 Ma and smaller peaks at 2300–1700 Ma and 2700–2400 Ma. The ages of the youngest detrital zircon grains from all metasediment samples fall in a relatively narrow range between 570 and 540 Ma and define late Neoproterozoic (Ediacaran) – early Cambrian maximum depositional ages. This is consistent with similar data (590–520 Ma), reported for metasediments from the Gissar and Kyzylkum segments of STS by Mirkamalov et al. (2012), Konopelko et al. (2015) and Worthington et al. (2017). The major Neoproterozoic peak, characteristic for all samples, is often subdivided into three smaller overlapping peaks at 1200–900 Ma, 900–700 Ma and 700–550 Ma with the two youngest peaks being predominant. Notably only the youngest peak at 700–550 Ma was registered in the Baisun metasediments (Fig. 7a) while the rocks from the Kyzylkum segment are characterized by broad Neoproterozoic peaks (Fig. 8). Another characteristic feature of the Baisun metasediments is a relatively large proportion of Neoarchean zircon grains (Fig. 7a), which is also typical for some Kyzylkum samples such as the mica schist of the Uchkuduktau Fm. (Fig. 8).

The distribution of detrital zircon ages from the Garm-Baisun-Kyzylkum samples, representing the Neoproterozoic basement of the Karakum continent, generally follows the distribution of zircon ages reported for the Precambrian basement of the Tarim Craton (Rojas-Agramonte et al., 2014; Han et al., 2015). This is illustrated in Fig. 8 where probability curves of detrital and magmatic zircon ages from the Tarim Craton and the Northern Tien Shan are shown for comparison. As seen in Fig. 8, the patterns of detrital zircon ages from the Kyzylkum and Baisun samples are similar to those from the Tarim Craton, characterized by major peak at 1100–750 Ma and additional peaks around 1800 and 2400 Ma. Similar peaks are also characteristic for the zircon age spectra from the Northern Tien Shan (Fig. 8). However, as it was noted by Han et al. (2015), the Grenvillian ages in the range 1600–1200 Ma, forming a major peak in the Northern Tien Shan age pattern (Fig. 8), are almost ubiquitously absent in the Precambrian Tarim basement and increasing proportion of the Grenville-age zircon grains in the lower-middle Paleozoic sediments of the Tarim cover is explained by their derivation from Grenvillian terranes located to the north of Tarim. Thus, Precambrian detrital zircon grains in Ediacaran – early Paleozoic sediments, comprising the basement of the western South Tien Shan – Karakum, were probably derived from the southern Precambrian continents of Karakum and Tarim, which experienced a 1200–750 Ma orogeny (cf. He et al., 2014). Transport of sediments from the Northern Tien Shan and Paleo-Kazakhstan was limited as indicated by the absence of the Grenville-age zircon population that is specifically characteristic for these terranes. Limited transport from the north can be explained by relative positions of the Karakum and Paleo-Kazakhstan in the Neoproterozoic and early Paleozoic times when these terranes were separated by oceanic basins and major volcanic arcs, which hampered the transport of sediments from the north but provided clastics with 800–500 Ma ages due to rapid uplift and erosion (cf. Konopelko and Klemd, 2016; Konopelko et al., 2014, 2017b).

7.2. Geochronology of the Baisun block and tectonic setting of Barrovian metamorphic complexes of South Tien Shan

Four geochronologically investigated magmatic rocks from the Baisun block include two anatectic granites, associated with migmatized gneisses, and two clearly post-metamorphic rocks, thus, representing the rock types, which are important for understanding the metamorphic and magmatic evolution of the area. The four samples yielded ages in the range 352–323 Ma. An anatectic granite, associated with migmatized gneisses of the Sangardak river valley, which formed as a result of crustal melting during high-grade metamorphism, yielded an age of 340 ± 5 Ma (sample 8). A mafic porphyritic dike (sample 5) crosscutting the anatectic granite yielded a 339 ± 3 Ma age, which is indistinguishable from the age of the surrounding granite within error limits. An older and somewhat poorly defined age of ca. 352 Ma was obtained for porphyritic granite from the same area (sample 7).

The metamorphic rocks and the anatectic granites of the Baisun block are overlain by thick Carboniferous volcanic formations of rift affinity. Early Carboniferous (Visean) paleontological ages of the Zoi Fm. (Abduazimova, 2001), which unconformably overlies the metamorphic basement, constrain the age of Barrovian metamorphism at Baisun as pre-Serpukhovian. This is in agreement with 352–340 Ma ages of anatectic granites suggesting an early Carboniferous age of the peak metamorphism. A 339 ± 3 Ma age, obtained for an unmetamorphosed mafic dike crosscutting the anatectic granite, may indicate rapid exhumation of the metamorphic rocks prior to onset of rift-

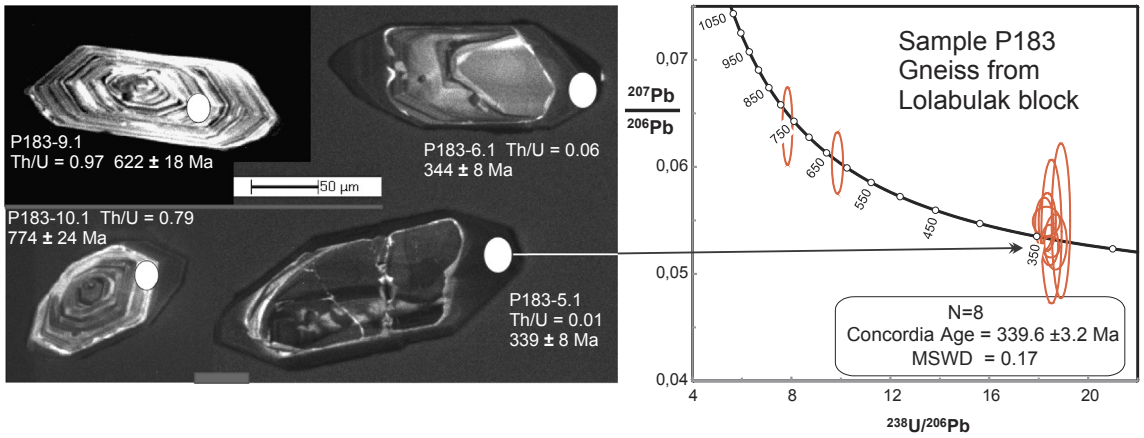

Fig. 10. Representative CL images of analyzed zircon and U-Pb analytical data for the Lolabulak gneiss (after Mirkamalov et al., 2012).

related volcanism. Magmatic activity associated with rifting continued during the Carboniferous and we interpret the 323 Ma old Ushor monzodiorite to represent a group of intrusions, which are comagmatic with volcanics of the overlying Vakhshivar Fm. with Serpukhovian paleontological age.

The Silurian and Devonian ages of the Baisun granites that are shown on geological maps (Shayakubov, 1998) are in conflict with the Carboniferous intrusive ages that are reported in the present study. However, the obtained Carboniferous ages are in agreement with recently reported data for the Lolabulak and Garm blocks where the age of metamorphism and crustal melting was constrained by SHRIMP dating of metamorphic zircon rims (Mirkamalov et al., 2012; Konopelko et al., 2015). Although datable zircon overgrowth was not identified in the metamorphic rocks studied here, the ages that were obtained from the Baisun anatectic granites are similar to the 340 Ma age of metamorphism reported from gneiss from the adjacent Lolabulak block by Mirkamalov et al. (2012). Because the preliminary publication of these authors did not provide any interpretation of metamorphic ages, we reproduce their zircon CL images with analytical spots, ages and Th/U ratios, as well as concordia diagram for the Lolabulak gneiss in Fig. 10.

On CL images, the zircon grains from the Lolabulak gneiss are characterized by bright oscillatory zoned cores and wide dark unzoned rims. Two analyses of cores yielded ages of 774 and 622 Ma and Th/U ratios 32–35 typical for magmatic zircon (Kirkland et al., 2015). The Neoproterozoic ages of the cores are similar to ages of detrital zircon grains from the Baisun metasediments (Fig. 10). The dark rims with low Th/U ratios (0.01–0.06), indicative of metamorphic zircon (Rubatto, 2002), are interpreted as zircon overgrowths during the peak metamorphism at Lolabulak. Eight analyses of rims plot as a tight cluster yielding a concordia age of 340 ± 3 Ma, which is indistinguishable from the age of anatectic granite from the Baisun block and similar to a ca. 330 Ma age of the older metamorphic event in the Garm block (Konopelko et al., 2015). Thus, the early Carboniferous (Visean) Barrovian metamorphism is proved to be a characteristic feature of the South Gissar unit where the Lolabulak, Baisun and Garm blocks form a 300 km long belt of regionally metamorphosed rocks (Fig. 2).

Konopelko et al. (2015,2018) interpreted the early Permian metamorphic event, recorded in the Garm and Alai blocks, as a result of crustal thickening during the late Paleozoic collision. However, in the early Carboniferous, the STS developed as a passive margin of the Turkestan Ocean while this margin was located at least 250 km north of the South Gissar unit as evidenced by the position of the South Tien Shan Suture (Fig. 2). Therefore, the early Carboniferous Barrovian metamorphism in the South Gissar was probably unrelated to the evolution of a passive margin. An alternative explanation can be suggested based on the character and position of the three major late Paleozoic suture zones in the area, which include the Kundajuaz, Gissar and Darvaz sutures, located in the Baisun block, south Gissar range and NW Pamirs, respectively (Fig. 1). The sutures are marked with ophiolites and associated with early-middle Carboniferous magmatic belts (Konopelko et al., 2017a). Plagiogranites and volcanics from the Darvaz zone were recently dated by Frölich et al. (2018) and yielded ages in the range 355–346 Ma, which are similar to ages obtained for the Baisun granites in the present study. The three sutures form a large semicircle bordering the Tajik depression from the north. The orientation of the NNE striking Kundajuaz and Darvaz sutures is markedly different from the east–west stretching Tien Shan structures. Geophysical data indicate that similar NNE striking ophiolite belts may be located under the sedimentary cover of the Tajik depression (Kuhtikov, 1981). In contrast to linear latitudinal Tien Shan structures, which formed as a result of frontal continental collision, relatively small tectonic blocks of the South Gissar, separated by several suture zones, resemble a typical archipelago pattern. This archipelago with multiple subduction zones was probably positioned between the larger continents of Karakum and Tarim and was possibly connected with the Paleotethys Ocean located to the south. The archipelago scenario can explain hot and rapid metamorphic and tectonic processes in the South Gissar during Carboniferous as it has been shown for the ongoing (ca. 23 Ma–present) collision between the Eurasian, Australian, and Philippine Sea plates in Indonesia (Hall, 2011; Hall and Sevastjanova, 2012). In the Indonesian archipelago convergence has been accommodated by a complex tectonic system of multiple subduction zones in which subduction rollback drove multiple synchronised episodes of high-temperature extension and fragmentation of microcontinents accompanied by ultrahigh-temperature metamorphism and crustal melting that was followed by rapid exhumation of metamorphic rocks (Pownall et al., 2013, 2014). Pownall et al. (2016) emphasized that the Indonesian archipelago is a rare modern example of rapid extension and exhumation of highly metamorphosed rocks that can help to understand similar processes, described in several older metamorphic terranes, which, in our opinion, can be also applied to the Carboniferous Barrovian metamorphism in the South Gissar.

7.3. Late Carboniferous basalts in northern Kyzylkum

Because metabasalts comprise a noticeable component of the STS Neoproterozoic basement formations they were systematically sampled for geochronological investigations. However, only two samples from the northern Kyzylkum produced datable zircon populations: the metabasalt assigned to the Uchkuduktau Fm. of inferred Neoproterozoic age and the diabase dike associated with basalts of the Elemesashchy Fm. Surprisingly, both rocks yielded late Carboniferous crystallization ages in the range 320–300 Ma (samples 218 and 16,183 in Fig. 9). In addition, the Elemesashchy diabase produced a population of rounded

xenogenic zircon with significant proportion of 490–450 Ma grains (Fig. 9). These ages are similar to a 438 Ma age of the adjacent Teskuduk ophiolite (Dolgopolova et al., 2017) and provide additional information on magmatic events, associated with the early stages of the evolution of the Turkestan Ocean.

The origin, extent and tectonic setting of the newly found late Carboniferous mafic magmatic pulse in northern Kyzylkum are not clear and shall be given special attention in the future. However, finding a late Carboniferous metabasalt among the metamorphosed sediments assigned to Neoproterozoic age may indicate that the so-called Caledonian basement of the Kyzylkum segment has a complicated structure and includes nappes of younger rocks juxtaposed with Neoproterozoic formations in a mega-mélange (cf. Sabdushev and Usmanov, 1971). It also means that the regional greenschist-facies metamorphism, post-dating the thrusting, is younger than the ca. 300 Ma crystallization age of the basalt, which is in agreement with ca. 280 Ma Ar-Ar mica and U-Pb apatite ages reported for the adjacent area around the giant Muruntau gold deposit (Wilde et al., 2001; Glorie et al., 2019).

8. Conclusions

Age spectra of detrital zircon grains from metasediments of Kyzylkum and Baisun show remarkable similarities over the whole western part of the South Tien Shan terrane. The 570–540 Ma ages of the youngest grains define late Neoproterozoic (Ediacaran) – early Cambrian maximum depositional ages of the metasediments. All samples are characterized by a major Neoproterozoic peak at 1200–600 Ma and smaller peaks at 2300–1700 and 2700–2400 Ma. This age pattern is similar to that reported for the Precambrian basement of the Tarim Craton and contrastingly different from the Northern Tien Shan where 1600–1200 Ma (Grenville-age) zircon population is a dominant feature. Thus, detrital zircon grains in Ediacaran sediments, comprising the basement of the western South Tien Shan terrane, were derived from the southern Precambrian continents of Karakum and Tarim while transport from the north was limited. The finding a late Carboniferous metabasalt among the metasediments in northern Kyzylkum may indicate that the South Tien Shan basement has a complicated structure and includes nappes of younger rocks juxtaposed with Neoproterozoic formations in a mega-mélange.

The age of the Barrovian metamorphism in the Baisun block is constrained by the 352–340 Ma ages of anatectic granites, corresponding to the early Carboniferous. These ages are in agreement with the 340–330 Ma SHRIMP ages of metamorphic zircon overgrowths that were established for the adjacent Lolabulak and Garm metamorphic blocks. Based on the distribution of suture zones we suggest that during the Carboniferous the relatively small tectonic blocks of the South Gissar comprised an archipelago, located to the south or between the larger continents of Karakum and Tarim and possibly connected with the Paleotethys Ocean. The archipelago scenario can explain hot and rapid metamorphic and tectonic processes, documented in the South Gissar, similar to the ongoing collision along the Australia – SE Asia junction.

Conflict of interest

The authors declared that there is no conflict of interest.

Acknowledgements

We are grateful to Farid Divaev for his generous assistance in the field. Robert Anczkiewicz provided access to laboratory facilities in Kraków. Sergey Petrov and Yuliya Mun were involved in sample preparation and analytical work. Comments of two anonymous reviewers helped to improve original version of the manuscript. The work was supported by the Ministry of Education and Science of the Russian Federation (project No 14.Y26.31.0018 – I.S., D.K., P.K.). D. Konopelko acknowledges travel grant from SPbGU (C0LLAB2019_2, Id: 37752801) and support through the Natural History Museum, London where part of the study was carried out in the frame of Research Fellowships at the Centre for Russian and Central EurAsian Mineral Studies (CERCAMS). Part of the research was conducted on the state assignment of IGM SB RAS, Ministry of Education and Science, RF. This is a contribution to IGCP 662 Project “Orogenic Architecture and Crustal Growth from Accretion to Collision” under the patronage of UNESCO-IUGS.

Appendix A. Zircon LA-ICP-MS analyses

The zircons were separated using conventional methods. Selected zircon grains were handpicked and mounted in epoxy resin together with chips of standard zircon grains. The grains were polished down to about half of their thickness. Prior to analysis, the zircon grains were documented utilizing a scanning electron microscope equipped with CL detector at the Natural History Museum, London. The U–Th–Pb isotope analyses were carried out in the laboratories of the Hong Kong and Nanjing Universities, China and at the Kraków Research Centre, Poland.

At the Department of Earth Sciences of Hong Kong University, the zircon U–Pb dating was conducted applying a Nu Instruments MC-ICP-MS with a Resonetics Resolution M-50-HR Excimer Laser Ablation System. Analyses were performed with a beam of 30 μm in diameter and 6 Hz repetition rate, generating a signal intensity of 4 mV at mass ^{238}U for the standard zircon 91,500. Typical ablation time is 40 s, resulting in pits of ca. 30–40 μm in depth. Masses of ^{238}U, ^{232}Th, ^{208}Pb, ^{207}Pb, ^{206}Pb, ^{204}Pb were measured simultaneously in a static-collection mode. Zircons 91,500 (1065.4 ± 0.3 Ma, Wiedenbeck et al., 1995) and GJ-1 (609 Ma, Jackson et al., 2004) were used as external standards and each was analyzed twice with every 10 analyses of the unknown samples. The detailed operation conditions and procedures followed Xia et al. (2011). Off-line signal selection, quantitative calibration, and time-drift correction were processed by software ICPMSDataCal (Liu et al., 2010).

At the State Key Laboratory for Mineral Deposits Research of Nanjing University, the zircon U-Pb dating was carried out by using Agilent 7500 s ICP-MS coupled to a New Wave 213 nm LA system. The laser beam is 24 μm in diameter and the repetition rate is 5 Hz. The detailed instrumental procedures follow Jackson et al. (2004). The raw data were calculated by the software package GLITTER version 4.4 (http://www.glitter-gemoc.com/) and the common lead correction was conducted with the program ComPbCorr#3 15G (Andersen, 2002).

At the Kraków Research Centre, the zircon U–Pb dating was conducted utilizing a 193 μm excimer laser RESOlution M-50 by Resonetics. The laser ablation system was coupled with a quadrupole ICP-MS XSeriesII by Thermoelectron. Zircon standards 91,500 (1065.4 ± 0.3 Ma, Wiedenbeck et al., 1995) and GJ-1 (609 Ma, Jackson et al., 2004) were used as external standards. Each individual analysis was preceded by 30 s measurement of instrumental background with the settings identical to those applied during ablation. The detailed instrumental procedures follow Jackson et al. (2004). Data reduction was conducted using Iolite v. 3.0 which runs within Wavemetrics Igor Pro software and followed the procedures described in Paton et al. (2011). Concordia diagrams and probability density plots were made using Isoplot 4.15 (Ludwig, 2008).

Appendix B. Supplementary material

Supplementary data to this article can be found online at https://doi.org/10.1016/j.jseaes.2019.03.025.

References

Abduazimova, Z.M. (Ed.), 2001. Stratigraphical dictionary of Uzbekistan. IMR Publishing House, Tashkent, pp. 580 (in Russian).

Akhmedjanov, M.A., Abdullayev, R.N., Borisov, O.M., Bazarbayev, E.R., Mirkhodjayev, I.M., Khokhlov, V.A., 1975. Precambrian of the Middle and South Tien Shan. Fan Tashkent (in Russian).
Andersen, T., 2002. Correction of common lead in U-Pb analyses that do not report ^{204}Pb. Chem. Geol. 192, 59–79.
Baratov, R.B. (Ed.), 1976. Subdivisions of Stratified and Intrusive Rocks of Tajikistan. "Donish" Publishing House, Dushanbe, pp. 269 (in Russian).
Biske, Y.S., 1996. Paleozoic Structure and History of Southern Tian-Shan. S.-Peterburg University Publishing House, St. Petersburg, pp. 190 (In Russian).
Biske, Yu.S., Seltmann, R., 2010. Paleozoic Tian-Shan as a transitional region between the Rheic and Urals-Turkestan oceans. Gondwana Res. 17, 602–613.
Biske, Yu.S., Konopelko, D., Seltmann, R., 2013. Geodynamics of the Late Paleozoic magmatism of Tien Shan and surrounding territories. Geotectonics 47 (4), 291–309.
Black, L.P., Jagodzinski, E.A., 2003. Importance of establishing sources of uncertainty for the derivation of reliable SHRIMP ages. Aust. J. Earth Sci. 50, 503–512.
Black, L.P., Kamo, S.L., Allen, C.M., Aleinikoff, J.N., Davis, D.W., Korsch, R.J., Foudoulis, C., 2003. TEMORA 1: a new zircon standard for U-Pb geochronology. Chem. Geol. 200, 155–170.
Bukharin, A.K., Maslennikova, I.A., Pyatkov, A.K., 1985. Pre-Mesozoic structural and facial zones of western Tian-Shan. "Fan" Publishing House, Tashkent, pp. 152.
Burtman, V.S., 2012. Tian Shan and High Asia: Geodynamics in the Cenozoic. GEOS, Moscow, pp. 188 (in Russian).
Burtman, V.S., 2015. Tectonics and geodynamics of the Tian Shan in the middle and late Paleozoic. Geotectonics 49 (4), 302–319.
Cai, K., Long, X., Chen, H., Sun, M., Xiao, W., 2018. Accretionary and collisional orogenesis in the south domain of the western Central Asian Orogenic Belt (CAOB). J. Asian Earth Sci. 153, 1–8.
Dolgopolova, A., Seltmann, R., Konopelko, D., Biske, Yu.S., Shatov, V., Armstrong, R., Belousova, E., Pankhurst, R., Koneev, R., Divaev, F., 2017. Geodynamic evolution of the western Tien Shan, Uzbekistan: insights from U-Pb SHRIMP geochronology and Sr-Nd-Pb-Hf isotope mapping of granitoids. Gondwana Res. 47, 76–109.
Frölich, S.A., Gulzar, A.M., Ratschbacher, L., 2018. LA-ICP-MS U-Pb zircon and ^{40}Ar/^{39}Ar mica dating of igneous and metaigneous rocks from the Hindu Kush/Pamir (Badakhshan, Afghanistan). In: 16th International Conference on Thermochronology, Conference Abstracts, pp. 61.
Ghes, M.D., 2008. Terrane Structure and Geodynamic Evolution of the Caledonides of Tian-Shan. Altyn Tamga Publishing House, Bishkek, pp. 158 (in Russian).
Glorie, S., Jepson, G., Konopelko, D., Mirkamalov, R., Meeuws, F., Gilbert, S., Gillespie, J., Collins, A.S., Xiao, W., Dewaele, S., De Grave, J., 2019. Thermochronological and geochemical footprints of post-orogenic fluid alteration recorded in apatite: implications for mineralisation in the Uzbek Tian Shan. Gondwana Res. https://doi.org/10.1016/j.gr.2019.01.011.
Golovanov, I.M., 2001. Ore Deposits of Uzbekistan. GID-ROINGEO. Publishing House, Tashkent, pp. 611 (in Russian).
Hall, R., 2011. Australia–SE Asia collision: plate tectonics and crustal flow. In: Hall, R., Cottam, M.A., Wilson, M.E.J. (Eds.), The SE Asian Gateway: History and Tectonics of the Australia–Asia Collision: London, Geological Society. Special Publication 355, p. 75–109.
Hall, R., Sevastjanova, I., 2012. Australian crust in Indonesia. Aust. J. Earth Sci. 59, 827–844.
Han, Y., Zhao, G., Sun, M., Eizenhöfer, P.R., Hou, W., Zhang, X., Liu, D., Wang, B., Zhang, G., 2015. Paleozoic accretionary orogenesis in the Paleo-Asian Ocean: insights from detrital zircons from Silurian to Carboniferous strata at the northwestern margin of the Tarim Craton. Tectonics 34, 334–351. https://doi.org/10.1002/2014TC003668.
He, Z.Y., Zhang, Z.M., Zong, K.Q., Xiang, H., Klemd, R., 2014. Metamorphic P-T–t evolution of mafic HP granulites in the northeastern segment of the Tarim Craton (Dunhuang block): evidence for early Paleozoic continental subduction. Lithos 196–197, 1–13.
Herrington, R.J., Achmedov, N.A., Charter, W.J., 2005. The Khandiza Zn-Pb-Cu-Ag VMS deposit: part of a new'Bathurst District' in southern Uzbekistan? In: Mao, J., Bierlein, F.P. (Eds.), Mineral Deposit Research: Meeting the Global Challenge. Springer, Berlin Heidelberg, pp. 615–618.
Jackson, S.E., Pearson, N.J., Griffin, W.L., Belousova, E.A., 2004. The application of laser ablation-inductively coupled plasma-mass spectrometry to in situ U-Pb zircon geochronology. Chem. Geol. 211, 47–69.
Käßner, A., Ratschbacher, L., Pfänder, J.A., Hacker, B.R., Sonntag, B., Khan, J., Stanek, K.P., Zack, G., Gadoev, M., Oimahmadov, I., 2017. Proterozoic-Mesozoic history of the Central Asian orogenic belt in the Tajik and southwestern Kyrgyz Tian Shan: U-Pb, 40Ar/39Ar, and fission-track geochronology and geochemistry of granitoids. Geol. Soc. Am. Bull. 129, 281–303.
Konopelko, D., Klemd, R., 2016. Deciphering protoliths of the (U)HP rocks in the Makbal metamorphic complex, Kyrgyzstan: geochemistry and SHRIMP zircon geochronology. Eur. J. Mineral. 28 (6), 1233–1253.
Konopelko, D., Biske, G., Seltmann, R., Petrov, S.V., Lepekhina, E., 2014. Age and petrogenesis of the Neoproterozoic Chon-Ashu alkaline complex, and a new discovery of chalcopyrite mineralization in the eastern Kyrgyz Tien Shan. Ore Geol. Rev. 61, 175–191.
Konopelko, D., Klemd, R., Mamadjanov, Y., Hegner, E., Knorsch, M., Fidaev, D., Kern, M., Sergeev, S., 2015. Permian age of orogenic thickening and crustal melting in the Garm Block, South Tien Shan, Tajikistan. J. Asian Earth Sci. 113, 711–727.
Konopelko, D., Seltmann, R., Mamadjanov, Y., Romer, R.L., Rojas-Agramonte, Y., Jeffries, T., Fidaev, D., Niyozov, A., 2017a. A geotraverse across two paleo-subduction zones in Tien Shan, Tajikistan. Gondwana Res. 47, 110–130.
Konopelko, D., Klemd, R., Petrov, S.V., Apayarov, F., Nazaraliev, B., Vokueva, O., Scherstén, A., Sergeev, S., 2017b. Precambrian gold mineralization at Djamgyr in the Kyrgyz Tien Shan: - tectonic and metallogenic implications. Ore Geol. Rev. 86, 537–547.
Konopelko, D., Wilde, S.A., Seltmann, R., Romer, R.L., Biske, Yu.S., 2018. Early Permian intrusions of the Alai range: Understanding tectonic settings of Hercynian post-collisional magmatism in the South Tien Shan, Kyrgyzstan. Lithos 302–303, 405–420.
Kirkland, C.L., Smithies, R.H., Taylor, R.J.M., Evans, N., McDonald, B., 2015. Zircon Th/U ratios in magmatic environs. Lithos 212–215, 397–414.
Kuhtikov, M.M. (Ed.), 1981. The Earth crust and mantle of Tajikistan. Donish, Dushanbe, pp. 283 (in Russian).
Liu, Y., Gao, S., Hu, Z., Gao, C., Zong, K., Wang, D., 2010. Continental and oceanic crust recycling-induced melt-peridotite interactions in the Trans-North China Orogen: U-Pb dating, Hf isotopes and trace elements in zircons from mantle xenoliths. J. Petrol. 51, 537–571.
Lomize, M.G., Demina, L.I., Zarshchikov, A.A., 1997. The Kyrgyz-Terskei Paleo-oceanic Basin, Tien Shan. Geodyn. Ser. 6, 35–55.
Loury, C., Rolland, Y., Lanari, P., Guillot, S., Bosch, D., Ganino, C., Jourdon, A., Petit, C., Gallet, S., Monié, P., Riel, N., 2018. Permian charnockites in the Pobeda area: implications for Tarim mantle plume activity and HT metamorphism in the South Tien Shan range. Lithos. https://doi.org/10.1016/j.lithos.2018.01.025.
Ludwig, K.W., 2008. User's manual for Isoplot 3.70: A geochronological toolkit for Microsoft Excel. Berkeley Geochronology Center Special Publication Number 4 (Berkeley).
Mirkamalov, R.H., Chirikin, V.V., Khan, R.S., Kharin, V.G., Sergeev, S.A., 2012. Results of U-Pb (SHRIMP) dating of granitoid and metamorphic complexes of the Tien Shan fold belt (Uzbekistan). Vestnik SPbGU 7–1, 3–25 (in Russian).
Paton, C., Hellstrom, J., Paul, B., Woodhead, J., Hergt, J., 2011. Iolite: freeware for the visualisation and processing of mass spectrometric data. J. Anal. At. Spectrom. 26 (12), 2508–2518.
Pownall, J.M., Hall, R., Watkinson, I.M., 2013. Extreme extension across Seram and Ambon, eastern Indonesia: evidence for Banda slab rollback: Solid. Earth 4, 277–314.
Pownall, J.M., Hall, R., Armstrong, R.A., Forster, M.A., 2014. Earth's youngest known ultrahigh-temperature granulites discovered on Seram, eastern Indonesia. Geology 42, 279–282.
Pownall, J.M., Hall, R., Lister, G.S., 2016. Rolling open Earth's deepest forearc basin. Geology 44, 947–950.
Popov, V.I., 1938. History if depressions and uplifts of the western Tien Shan. Committee of Sciences of UzSSR Publishing House, Tashkent, pp. 415 (in Russian).
Rojas-Agramonte, Y., Kröner, A., Alexeiev, D.V., Jeffreys, T., Khudoley, A.K., Wong, J., Geng, H., Shug, L., Semiletkin, S.A., Mikolaichuk, A.V., Kiselev, V.V., Yang, J., Seltmann, R., 2014. Detrital and igneous zircon ages for supracrustal rocks of the Kyrgyz Tianshan and palaeogeographic implications. Gondwana Res. 26, 957–974.
Rubatto, D., 2002. Zircon trace element geochemistry; partitioning with garnet and the link between U-Pb ages and metamorphism. Chem. Geol. 184, 123–138.
Sabdushev, S.S., Usmanov, R.R., 1971. Tectonic nappes, mélanges and ancient oceanic crust in Tamdytau (Western Uzbekistan). Geotectonika 5, 27–36.
Şengör, A.M.C., Natal'in, B.A., Burtman, V.S., 1993. Evolution of the Altaid tectonic collage and Paleozoic crust growth in Eurasia. Nature 364, 299–307.
Shayakubov, T.S. (Ed.), 1998. Geological Map of Uzbekistan, 1:500 000 Goskomgeologia, Tashkent (in Russian).
Shayakubov, T.S., Dalimov, T.N. (Eds.), 1998. Geology and Minerals of the Republic of Uzbekistan. "Universitet", Tashkent, p. 722. (in Russian).
Vlasov, N.G., Dyakov, Y.A., Cherner, E.S. (Eds.), 1991. Geological Map of the Tajik SSR and Adjacent Territories, 1:500 000, VSEGEI Leningrad-Saint Petersburg (in Russian).
Volkova, N.I., Budanov, V.I., 1999. Geochemical discrimination of metabasalt rocks of the Fan-Karategin transitional blueschist/greenschist belt, South Tianshan, Tajikistan: seamount volcanism and accretionary tectonics. Lithos 47, 201–216.
Wiedenbeck, M., Alle, P., Corfu, F., Griffin, W.L., Meier, M., Oberli, F., Quadt, A., Roddick, J.C., Spiegel, W., 1995. Three natural zircon standards for U-Th–Pb, Lu–Hf, trace element and REE analyses. Geostand. Geoanal. Res. 19, 1–23.
Wilde, A.R., Layer, P., Mernach, T., Foster, J., 2001. The giant Muruntau deposit: geologic, geochronologic, and fluid inclusion constraints on ore genesis. Econ. Geol. 96, 633–644.
Windley, B.F., Alexeiev, D., Xiao, W., Kröner, A., Badarch, G., 2007. Tectonic models for accretion of the Central Asian Orogenic Belt. J. Geol. Soc. London 164, 31–47.
Worthington, J.R., Kapp, P., Minaev, V., Chapman, J.B., Mazdab, F.K., Ducea, M.N., Oimahmadov, I., Gadoev, M., 2017. Birth, life, and demise of the Andean – syn-collisional Gissar arc: Late Paleozoic tectono-magmatic-metamorphic evolution of the southwestern Tian Shan, Tajikistan. Tectonics 36. https://doi.org/10.1002/2016TC004285.
Xia, X., Sun, M., Geng, H., Sun, Y., Wang, Y., Zhao, G., 2011. Quasi-simultaneous determination of U-Pb and Hf isotope compositions of zircon by excimer laser-ablation multiple-collector ICPMS. J. Anal. At. Spectrom. 26, 1868–1871.
Zonenshain, L.P., Kuzmin, M.I., Natapov, L.M., 1990. Geology of the USSR: A Platetectonic Synthesis. AGU Geodynamics Series 21. American Geophysical Union, Washington, DC, pp. 242.